Indian J Phys
https://doi.org/10.1007/s12648-020-01842-z

ORIGINAL SCIENTIFIC RESEARCH

Influence of Na_2O addition on the alkali borochromate glasses: structure and ligand field

A Samir*

Engineering Mathematics and Physics Department, Faculty of Engineering at Shoubra, Benha University, Cairo 11629, Egypt

Received: 16 July 2019 / Accepted: 18 March 2020

Abstract: Trivalent chromium is a very common ion used for coloring in the industry of glass. As glasses are melted under high oxidizing circumstances, hexavalent chromium Cr(VI) can be fixed and found in certain advertising applications of UV-protection receptacles. Melt quenching technique is employed to prepare oxide glasses with a general formula $x$$Na_2O$–$(30 - x)$ Li_2O–10K_2O–10ZnO–49.7B_2O_3–0.3Cr_2O_3 (where x = 0, 5, 10 and 15 mol%). The amorphous nature of the samples is confirmed using X-ray diffraction. The optical absorption spectra have been recorded, and the resulting data were used for the ligand field theory analysis, from which the crystal-field energy (10Dq), Racah parameters (B and C) and nephelauxetic function (h) were evaluated. The variations in the optical bandgap and the band tail with Na_2O content have been discussed in relation to the glass structure. FTIR of these glasses revealed that the borate network is affected by the replacement of Na_2O by Li_2O content. It showed also reduction in N_4 with increasing Na_2O. This result indicates the increase of non-bridging oxygens (NBOs) which in turn reduces the rigidity of the glass matrix and opens up the structure. The density and the molar volume (V_M) measurements were also employed to investigate the structure. These measurements show a linear increase as Na_2O content increases. This can be attributed to the differences in the ionic radii of sodium and lithium ions, being larger for sodium. UV–Visible optical absorption spectra show three characteristics bands around ~ 588, 435 and 360 nm which are assigned to the transitions $^4A_{2g} \rightarrow {}^4T_{2g}$, $^4A_{2g} \rightarrow {}^4T_{1g}$ and $^4A_{2g} \rightarrow {}^2A_{1g}$, respectively. Racah parameters (B and C) show an opposite behavior. The obtained ratio (10Dq/B) reveals a strong ligand field around chromium ions. Also, the nephelauxetic parameter of the ligand shows the same 10Dq behavior. The increase of chromium ions in the trivalent state shows that it acts as modifiers, yielding the higher concentration of NBOs in the glass matrix and confirming the FTIR and optical results. Electron spin resonance spectroscopy was measured and studied to confirm the existence of Cr^{3+} and Cr^{6+}.

Keywords: Ligand field theory; Borochromate glasses; Optical properties; FTIR

1. Introduction

One of the most popular and the best glass former is B_2O_3, and it is found in nearly all commercially significant glasses. Boron is able to easily modify its coordination with oxygen three–four units so that it can compose adjustable structural units in glasses as well as in crystals [1, 2]. Alkali-borate glasses are highly transparent to visible light. In particular, the alkali oxide additives allow good mechanical stability and hygroscopic property of the glass network required for the working devices [3]. When adding a modifier such as ZnO to it, some units of BO_3 transform to BO_4 units up to a specific modifier level; after that, non-bridging oxygens are constructed by increasing the modifier content. At present, attention is given to examine glasses as valuable solid materials particularly those including a transition metal oxide as ZnO. Zinc oxide is a significant multifunctional material which is used in several applications because of its particular chemical, surface and tiny structural qualities [4]. The doped transition metal (TM) in glasses affect color and physical properties. The atomic number and the atomic weight of chromium are 24 and 51.996 g/mol, respectively. The chromium $3d^54s^1$ electron configuration is a paramagnetic transition metal ion. It is recognized that chromium has several oxidation states: Cr^{3+}, Cr^{4+}, Cr^{5+}, and Cr^{6+}. The Cr^{3+} state is the most dynamically and energetically stable state and is performing as a modifier in the matrix of

*Corresponding author, E-mail: ahmed.s2000@yahoo.com; ahmed.soliman01@feng.bu.edu.eg

Published online: 07 November 2020

glass. Cr^{6+} (d^0) has a closed shell configuration and is expected to strengthen the host glass network. The Cr^{3+} and Cr^{6+} ions doped in the glass system created a color in glasses which can be observed by UV–Vis spectra [5–7]. Specifically, paramagnetic chromium ions located in various glass matrices fulfill the requirements of varied prospective applications, like luminescence materials, solid-state lasers, and different electronic-optical devices [8–12]. The aim of this work is to study the effect of combining three alkali oxides (Na_2O, Li_2O and K_2O) in the Cr-doped zinc borate glasses using the experimental techniques like X-ray diffraction density (XRD), Fourier transform infrared spectroscopy (FTIR), UV–vis measurement to determine the structure and the optical properties of the investigated samples with varying amounts of Na_2O. This paper shows the correct position for the absorption edge for Cr-doped borate glasses.

2. Experimental details

Borochromate glasses of the composition $x$$Na_2O$–$(30 - x)$ Li_2O–$10K_2O$–$10ZnO$–$49.7B_2O_3$–$0.3Cr_2O_3$ (where $x = 0$, 5, 10 and 15 mol%) were prepared by melt quenching technique. Powders of these compounds in appropriate amounts were thoroughly mixed in an agate mortar and melted in porcelain crucibles at 1050 °C in an electrical furnace for ~ 1.5 h, in order to obtain bubble-free samples. Melts were shacked several times during heating to ensure a high degree of homogeneity, and then the melts were quenched between two polished copper blocks kept at room temperature to yield the homogeneous glasses. The amorphous natures of the glass samples were ensured from X-ray diffraction measurements (not shown). The prepared sample densities were estimated via carrying out the Archimedes principle using tetrachloride carbon as a submerging liquid. The sample's optical absorption spectra were reported in the spectral range 190–990 nm using JenWay-6405-type UV–VIS spectrophotometer. The ordinary absorption saturation in the UV zone was lessened through decreasing the glass segments thickness, or equivalently adjusting a slight proportion of the powder suspended in glycerin. All of the optical absorption spectra were obtained with a scanning average of 1 nm/s. The light spot is scanned over different parts of the sample to ensure the reproducibility of the spectra. Infrared absorption spectra in the range 4000–400 cm^{-1} were recorded using Thermo FTIR 200 spectrometer with a scanning rate of 75 cm^{-1}/s. In order to measure FITR, the powder samples were blended with very pure KBr and compressed into discs. The attribution of the sample-to-KBr was settled at ~ 3% for all samples. ESR spectra were recorded using an X-band EMX spectrometer (Bruker Germany) on the powder samples placed inside standard quartz tubes. The field modulation and the microwave power were set to 100 kHz and 10 mW, respectively, while the magnetic field was scanned in the range 75–6000 G. All measurements were recorded at room temperature.

3. Results and discussion

3.1. Optical basicity

The optical basicity (Λ) of an oxide medium is the average electron donor power of all the oxygen atoms comprising the medium. Theoretical optical basicity for the glass system was calculated by using the average electronegativity (χ_{av}) on the basis of the following equation proposed by Duffy [13] as follows:

$$\chi_{av} = \sum_i x_i \chi_i \quad (1)$$

$$\Lambda = \frac{0.75}{\chi_{av} - 1.35} \quad (2)$$

where x_i is the concentration percentage and X_i is the electronegativity of any oxide compound. The electronegativity of the pure elements was brought from the Allen scale table [14]. The estimated optical basicity values exhibit the opposite trend to the average electronegativity with increasing the concentration of Na_2O content as shown in Fig. 1. The increment of the optical basicity may be attributed to the lower electronegativity of the Na_2O than that of Li_2O, the increase in the optical basicity indicating overall decreasing covalency of the whole glass system [15–17].

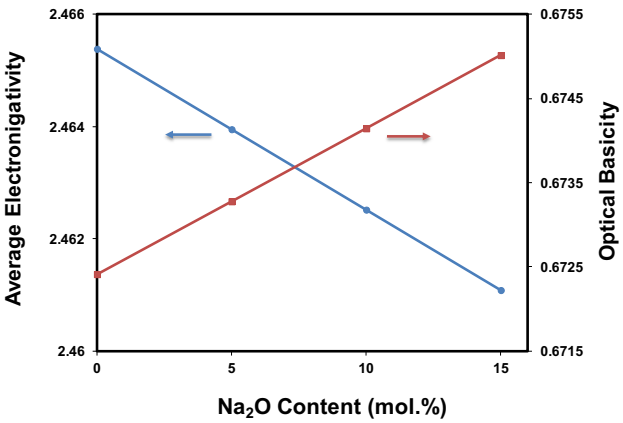

Fig. 1 The average electronegativity and the calculated optical basicity of the investigated samples

3.2. Density and molar volume

Generally, the density and the molar volume are prospected to present opposing behavior to each other, but the behavior differs in the current glasses. However, this irregular behavior was previously reported for several glass systems [18]. Figure 2 shows the behavior of this work. The increase in the density can be related to the replacement of Li_2O by Na_2O, and this can be interpreted as the molecular weight of Li_2O (29.88 g/mol) is less than that of Na_2O (61.97 g/mol). The increase of the molar volume with increasing the Na_2O content is most likely due to the replacement of smaller ionic radii ions (Li) by larger ionic radii ions (Na), resulted in a formation of excess free volume, which increases the overall molar volume of these glasses. This trend supports the so-called open structure concept [19, 20].

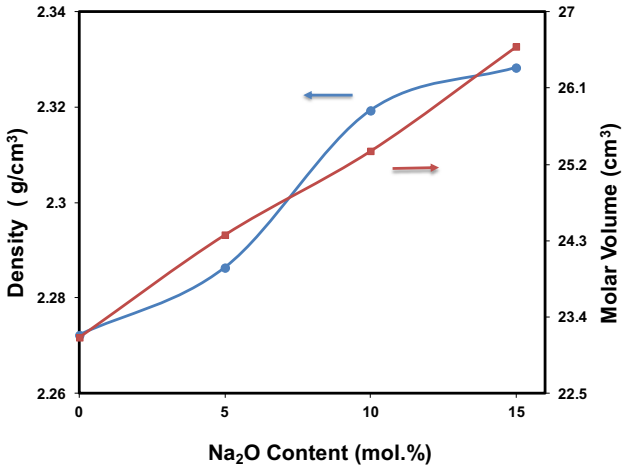

Fig. 2 Density and molar volume as a function of Na_2O content

3.3. FTIR analysis

Figure 3 shows the FTIR spectra of the investigated samples. Borate glass consists of three main regions, the first region located in the range 600–800 cm^{-1} is related to the B–O–B bending modes of (BO_3) units. The second region in the range 800–1200 cm^{-1} is related to the B–O bond stretching in (BO_4) units and the third one in the range 1200–1600 cm^{-1} is related to the stretching of the B–O in BO_3 units [21, 22]. The spectrum shows also an overlapped shoulder at $\sim$ 1650 cm^{-1} with the triangle BO_3 band which is due to the –OH bending vibration. Finally, a broad band is found around $\sim$ 3400 cm^{-1} due to the O–H vibration mode of water [8]. To explain the origin of this characteristic infrared symmetry, the spectra were deconvoluted using Gaussian components which give the best fit using the nonlinear least-squares fitting method. Figure 3 represents the N_4 ratio as a function of Na_2O content. N_4 (N_4 = area of BO_4/area of (BO_3 + BO_4)) and it is a factor used to measure the BO_4 creation ratio. The addition of Na_2O instead of Li_2O causes a decrease in the fraction of tetrahedrally coordinated boron atoms. The replacement of sodium ions by lithium ions leads to the conversion of tetrahedral BO_4 units to triangular BO_3 units with NBOs [2, 19, 23]. This means that the increase of NBOs becomes the dominant which tends to reduce the rigidity of the glass matrix. Hence, the glass becomes more open and the network becomes less tightly packed confirming the molar volume results.

3.4. Optical studies

Studying the fundamental absorption edge in the UV–Visible area is a helpful procedure for investigating the

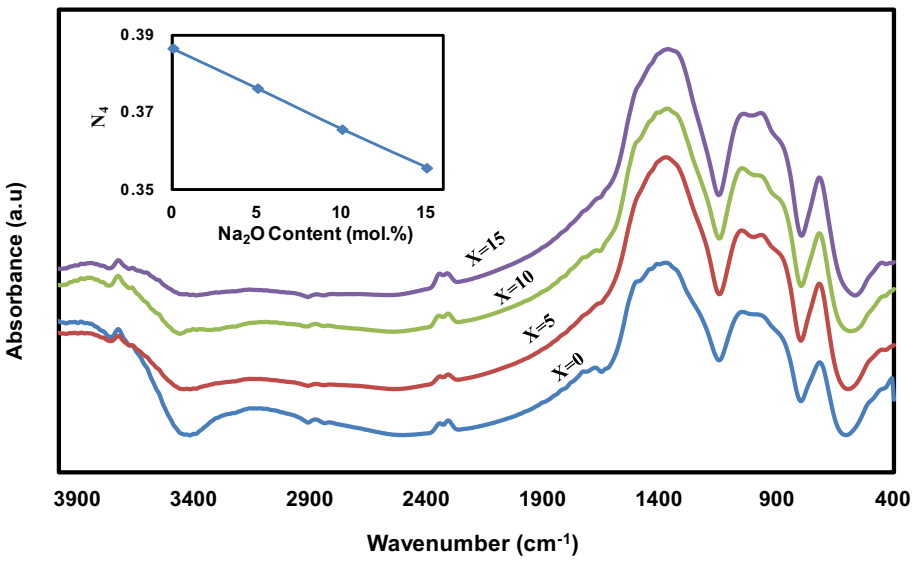

Fig. 3 FTIR spectra of all glassy samples (inset figure represents the N_4 ratio composition dependence)

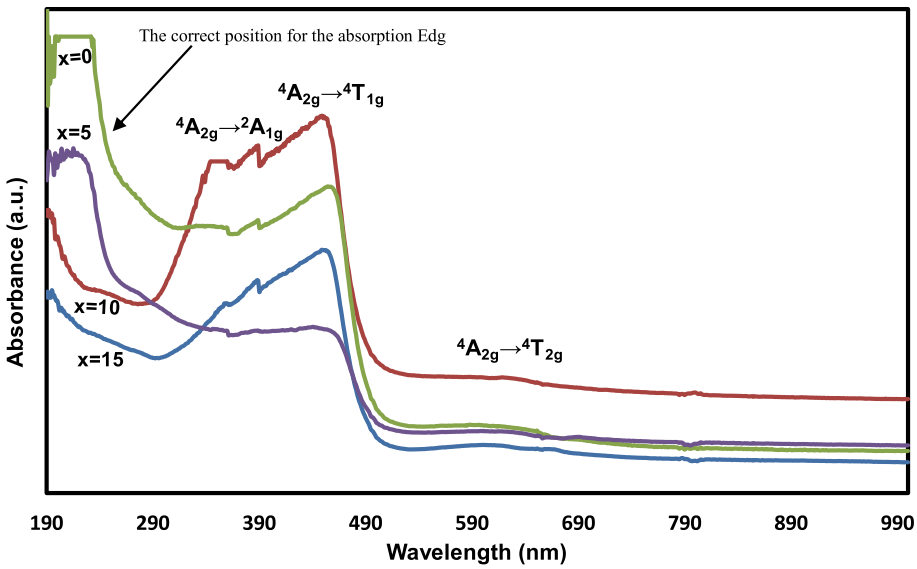

Fig. 4 UV–Visible absorbance of all samples doped with chromium oxide

optical transitions and the electronic band structure in crystalline as well as amorphous materials. The optical absorption spectra as a function of the wavelength of the chromium-doped glass samples observed at room temperature are shown in Fig. 4. The optical bandgap energy E_g was estimated according to equation [24–26]:

$$\alpha hv = B\,(hv - E_g)^n \tag{3}$$

The intercept was determined by extrapolating the straight line obtained by linear fitting at the linear section of the absorption edge. For the amorphous materials, the best fit of the absorption edge was obtained with $n = 2$, indicating an indirect allowed band transition model for the glassy samples. The E_g's were obtained from the observed absorption edges by drawing Urbach plots between $(\alpha hv)^{0.5}$ and photon energy (hv) (employing the indirect transitions model), and they are represented in Fig. 5. It is verified that the optical bandgap decreases (red shift) with an increase of the Na_2O content. This leads to create the excited states of localized electrons close to the conduction band of the glass samples. These localized levels interact with the conduction band and become more extended into the main bandgap [12, 27]. This might have shifted to the absorption edge to lower energy. This leads up to a significant reduction of the bandgap. Additionally, increasing the donor centers in the glass matrix tends to the higher concentration of non-bridging oxygens (NBOs) in the glass matrix [12, 27]. These results agree with the FTIR data.

The absorption coefficient in Urbach's exponential tail region is evaluated using the following equation [24–26]:

$$\alpha = \alpha_o \ \exp\ (hv/E_t) \tag{4}$$

where E_t is the band tail width. The values of Urbach energy or band tails width (E_t) were specified by taking the reciprocals of the slopes of the linear section of ln(α) and

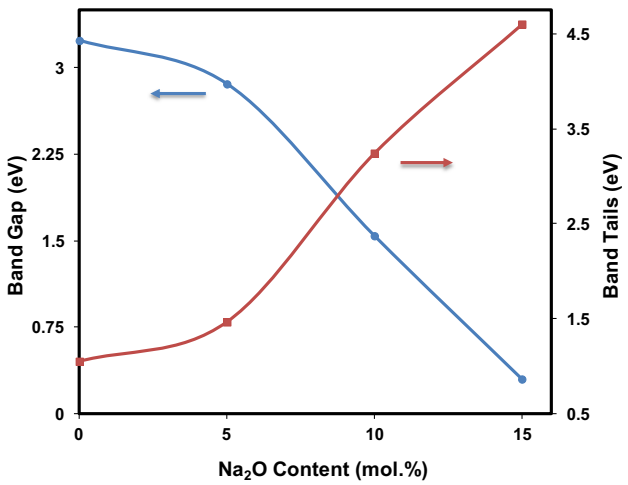

Fig. 5 Optical bandgap and optical band tails composition dependence

(hv) curves. The band tail width energy which corresponds to the width of the localized states is used to characterize the disorder limit in the amorphous. Figure 5, Table 1 shows the obtained values of E_t for all the investigated samples, which show the opposite behavior to optical bandgap energy. The increase in band tails width with Na_2O content could be due to the increased number of defects and the localization state in the forbidden gap.

On the other hand, the optical absorption studies of glasses doped with transition metals give rise to ligand field absorption energies, which reflect the distortion of the octahedral and tetrahedral co-ordinations. As presented in Fig. 4, the spectrum of the samples exhibits two main absorption bands at ~ 588 (υ_1) and 435 (υ_2) nm, which can be identified due to the conventional transitions of Cr^{3+} ions [28, 29]. A Tanabe–Sugano diagram can be used to

Table 1 The absorption transitions and optical parameters of chromium ions doped glasses

X (mol%)	Band positions (nm)			Optical parameters	
	Cr^{3+} Cr^{6+}				
	$^4A_{2g} \rightarrow {}^4T_{2g}$	$^4A_{2g} \rightarrow {}^4T_{1g}$	$^4A_{2g} \rightarrow {}^2A_{1g}$	E_g (eV)	E_t (eV)
0	587	433	370	3.23	1.04
5	588	433	363.5	2.86	1.46
10	592	435	361	1.54	3.24
15	595	435	358.5	0.29	4.60

identify the energy levels splitting in a d^3 electronic configuration. The spectra have been analyzed and the bands are assigned to $^4A_{2g} \rightarrow {}^4T_{2g}$ and $^4A_{2g} \rightarrow {}^4T_{1g}$ transitions, respectively, which refer to *d–d* transition of Cr^{3+} ion. The colors of the prepared samples are yellow green indicating a trivalent chromium oxidation state [28, 29]. Furthermore, Cr^{6+} ion is identified by the charge transfer absorption in the UV range around $\sim$ 360 (υ_3) nm. This band is attributed to $^4A2g \rightarrow {}^2A_{1g}$ transition, which is most likely due to the presence of contribution of the chromium ions in a higher valence state (Cr^{6+}), and it is not *d–d* transition [30–32]. The ligand field parameters, as crystal-field strength (10Dq) which represent the crystal-field splitting energy and the Racah parameters (B and C) which measure the inter-electronic repulsion among the 3d electrons of Cr^{3+} ion, have been evaluated from the spectral band absorption positions (υ_1, υ_2, υ_3 in cm^{-1} units) according to the following relations [9, 33–36]:

$$10Dq = v_1 \tag{5}$$

$$B = \frac{1}{3}\frac{(2v_1 - v_2)(v_2 - v_1)}{(9v_1 - 5v_2)} \tag{6}$$

$$C = \frac{(v_3 - 4B - 10Dq)}{3} \tag{7}$$

The obtained values of ligand field parameters are listed in Table 2. It is clear that the 10Dq shows a decrease with increasing Na_2O content due to the increase of the NBOs ratio of the investigated samples. Figure 6 represents the deconvolution which was made to identify the correct

Table 2 Ligand field parameters of chromium ions doped glasses

X (mol%)	Ligand field parameters					*h*
	10Dq (cm^{-1})	*B* (cm^{-1})	*C* (cm^{-1})	*C*/*B*	10Dq/B	
0	17,036	586	2549	4.35	2.91	1.724
5	17,007	589	2715	4.61	2.88	1.704
10	16,892	592	2814	4.76	2.86	1.693
15	16,807	603	2892	4.80	2.79	1.635

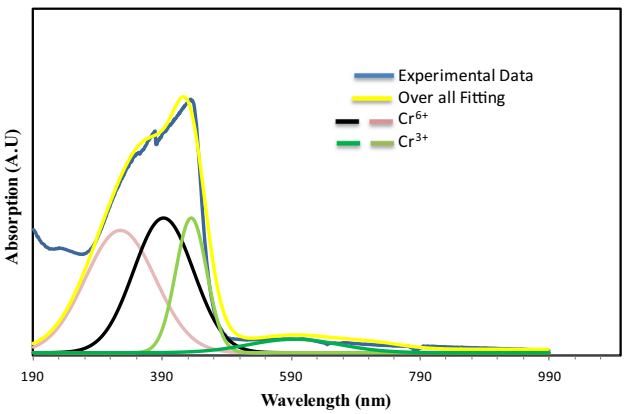

Fig. 6 UV–Visible absorption spectra for glass sample x = 15 mol% and the deconvolution procedure applied to it

positions for Cr^{6+} and Cr^{3+}. The variation of 10Dq with Na_2O content is represented in Fig. 7; the B and C parameters exhibit opposite behavior according to Table 2. The ratio 10Dq/B describes the crystal-field strength. In the strong crystal-field sites, the value of 10Dq/B greater than 2.3; whereas, in the weak field, it is much less than 2.3. Finally, in the intermediate fields, the 10Dq/B ratio is close to 2.3 value [36]. The obtained value of the ratio 10Dq/B reflects the strong crystal-field strength around chromium ions. Additionally, the Racah parameters are used in

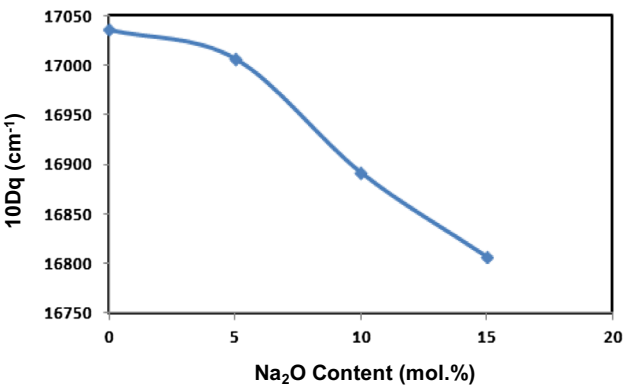

Fig. 7 Variation of 10Dq with compositions for the investigated samples

defining the degree of iconicity of the ligand bonding. The bonding formation (or nephelauxetic ratio h) was also evaluated using the following formula [8, 9]:

$$h = \frac{(B_{\text{free}} - B)/B_{\text{free}}}{k_{Cr^{3+}}} \quad (8)$$

where $B_{\text{free}} = 918\ \text{cm}^{-1}$ which represents the value of the free (gaseous) Cr^{3+} ion, and is the central metal ion, where its value is k_{Cr}^{3+} equal to 0.21. The obtained values of h for all the investigated glasses show the same behavior as 10Dq as presented in Table 2. It can be attributed to some of the Cr^{6+} ions which converted to the Cr^{3+} ions, reflecting an increase of the degree of covalency between Cr^{3+} and the surrounding ion [9]. The increasing of chromium ions in the Cr^{3+} state acts as modifiers, yielding the higher concentration of NBOs in the glass matrix [37, 38]. These assumptions are in complete agreement with the optical basicity behavior and FTIR results.

3.5. ESR studies

Figure 8 represents the ESR spectra for the investigated samples. The normalization was made to the spectra with respect to their mass in order to obtain appropriate comparison among the different samples. The normalized ESR spectra exhibit a significant dependence on Na_2O contents. At a low magnetic field, ESR spectra show two signals with effective g values at $g = 4.81$ and $g = 4.10$. The observed resonance signal at $g = 4.81$ can be attributed to the isolated Cr^{3+} ions in the strong ligand field sites whereas the second signal observed at $g = 4.10$ is mainly due to Cr^{3+} ions [39, 40]. The intensity of the signal at $g = 4.10$ decreases with the addition of Na_2O. The decrease is a result of the decrease of Li at the expense of Na ratio. But, the signal at $g = 4.81$ is slightly decreased. By comparing with Cr^{3+} optical absorption spectra, it is clear that the transition with $g = 4.81$ originates from υ_1 band (i.e., $\sim$ 588 nm) while the transition with $g = 4.10$ originates from υ_2 band (i.e., $\sim$ 435 nm). At the high field, ESR spectra exhibit three signals with effective g values at $g = 2.18$, $g = 2.03$ and $g = 1.93$. The observed signals at $g = 2.18$ and $g = 2.03$ are mainly due to the exchange of the coupled pairs or the large Cr^{3+} clusters. Their intensities are increased remarkably with increasing alkali oxide contents (Na_2O), in agreement with the υ_1 optical transition. Moreover, the sharp signal observed at $g = 1.93$ has been due to Cr^{6+} ions in agreement with the υ_3 optical transition. Evidently, both of the two signals at $g = 4.10$ and $g = 1.93$ have the same spectral shape, raising the possible contribution from both Cr^{3+} and Cr^{6+} to the $g = 4.10$ resonance [40].

4. Conclusion

Besides the usual Cr^{3+} absorption bands, additional UV Cr^{6+} transitions were identified. The separation between these transitions was performed through Na_2O additives, and the correct position for the absorption edge for Cr-doped borate glasses was obtained. The results of FTIR and the ligand field parameters revealed that the replacement of Na_2O on the bases of Li_2O causes a higher concentration of NBOs in the glass matrix. Finally, optical bandgap energy values decrease with the increasing of Na_2O content as well as the band tails' width exhibits the opposite trend indicating an increase in the density of the localized state. ESR spectroscopy confirmed the existence of both Cr^{6+} and Cr^{3+} oxidation states.

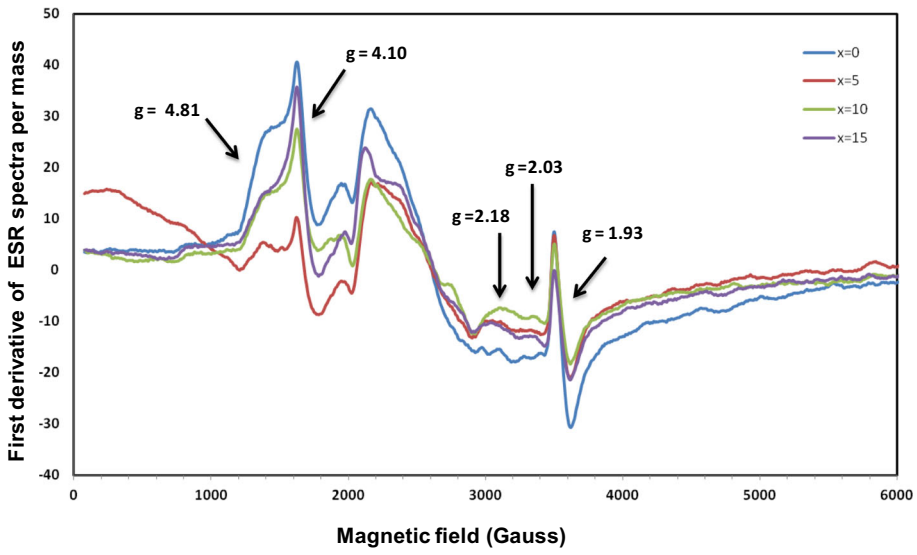

Fig. 8 ESR spectra for the investigated samples

References

[1] G Krishna Kumari et al *Mater. Res. Bull.* **47** 2646 (2012)
[2] Subhashini, H D Shashikala and N K Udayashankar *J. Alloys Compd.* **658** 996 (2016)
[3] A Edukondalu et al *J. Non Cryst. Solids* **358** 2581 (2012)
[4] G P Singh, S Kaur, P Kaur, S Kumar and D P Singh *Physica B* **406** 1890 (2011)
[5] P Meejitpaisan, J Kaewkhao, P Limsuwan and C Kedkaew *Procedia Eng.* **32** 787 (2012)
[6] R Vijay, P Ramesh Babu, V Ravi Kumar, M Piasecki, D Krishna Rao and N Veeraiah *Mater. Sci. Semicond. Process.* **35** 96 (2015)
[7] B Lakshmana Rao, Y N Ch Ravi Babu and S V G V A Prasad *J. Non Cryst. Solids* **382** 99 (2013)
[8] M A Hassan *J. Alloys Compd.* **574** 391 (2013)
[9] F Ahmad *J. Alloys Compd.* **586** 605 (2014)
[10] H Wen and P A Tanner *J. Alloys Compd.* **625** 328 (2015)
[11] A R Molla et al *J. Alloys Compd.* **583** 498 (2014)
[12] F S De Vicente, F A Santos, B S Simoes, S T Dias and M Siu Li *Opt. Mater.* **38** 119 (2014)
[13] J A Duffy *J. Non Cryst. Solids* **297** 275 (2002)
[14] L C Allen *J. Am. Chem. Soc.* **111** 9003 (1989)
[15] A Terczyñska-Madej, K Cholewa-Kowalska and M Laczka *Opt. Mater.* **33** 1984 (2011)
[16] J-J He, S-Y Wu, L-J Zhang, Y-Q Xu and C-C Ding *J. Non Cryst. Solids* **437** 58 (2016)
[17] Yusub, Ch Rajyasree, A Ramesh Babu, P M Vinaya Teja and D Krishna Rao *J. Non Cryst. Solids* **364** 62 (2013)
[18] M Farouk, A Samir, F Metawe and M Elokr *J. Non Cryst. Solids* **371** 14 (2013)
[19] Y B Saddeek, E R Shaaban, E Moustafa and H M Moustafa *Phys. B* **403** 2399 (2008)
[20] R D Shannon *Acta. Cryst. A* **32** 751 (1976)
[21] B Sailaja, R Joyce Stella, G Thirumala Rao, B Jaya Raja, V Pushpa Manjari and R V S S N Ravikumar *J. Mol. Struct.* **1096** 129 (2015)
[22] R Ciceo-Lucacel and I Ardelean *J. Non Cryst. Solids* **353** 2020 (2007)
[23] G Vijaya Prakash, D Narayana Rao and A K Bhatnagar *Solid State Commun.* **119** 39 (2001)
[24] A Samir, M A Hassan, A Abokhadra, L I Soliman and M Elokr *Opt. Quant. Electron.* **51** 123 (2019)
[25] M Farouk, A Samir and M El Okr, *Phys. B* **530** 43 (2018)
[26] M Farouk, F Ahmad and A Samir *Opt. Quant. Electron.* **51** 292 (2019)
[27] G Murali Krishna, B Anila Kumari, M Srinivasa Reddy and N Veeraiah *J. Solid State Chem.* **180** 2747 (2007)
[28] R V S S N Ravikumar, J Yamauchi, A V Chandrasekhar, Y P Reddy and P Sambasiva Rao *J. Mol. Struct.* **740** 169 (2005)
[29] M A Hassan, M Farouk, A H Abdullah, I Kashef and M M ElOkr *J. Alloys Compd.* **539** 233 (2012)
[30] Cz Koepke, K Wisniewski and M Grinberg *J. Alloys Compd.* **341** 19 (2002)
[31] Cz Koepke, K Wi´sniewski, M Grinberg and F Rozpłoch *J. Phys. Condens. Matter* **14** 11553 (2002)
[32] S Morimoto, S Khonthon and Y Ohishi *J. Non Cryst. Solids* **354** 3343 (2008)
[33] W A Pisarski, J Pisarska, G Dominiak-Dzik and W Ryba-Romanowski *J. Alloys Compd.* **484** 45 (2009)
[34] G Calas, O Majerus, L Galoisy and L Cormier *Chem. Geol.* **229** 218 (2006)
[35] M R Reddy, M S Reddy and N Veeraiah *Indian J. Pure Appl. Phys.* **44** 446 (2006)
[36] A B P Lever, *Inorganic Electronic Spectroscopy*, 2nd Edition (Amsterdam: Elsevier Science Publisher) (1986)
[37] G Naga Raju, N Veeraiah, G Nagarjuna and P V V Satyanarayana *Phys. B* **373** 297 (2006)
[38] G Little Flower, M Srinivasa Reddy, G Sahaya Baskaran and N. Veeraiah *Opt. Mater.* **30** 357 (2007)
[39] S Vijay, G Sivaramaiah, J L Rao and Kim *Mater. Res. Bull.* **60** 397 (2014)
[40] M A Hassan, F M Ebrahim, M G Moustafa, Z M Abd El-Fattah and M M El-Okr *J. Non Cryst. Solids* **515** 157 (2014)